Leaky-wave antenna with switchable omnidirectional conical radiation via polarization handedness

Liu, Yahong; Li, Meize; Song, Kun; Hu, Dingshan; Liu, Hongchao; Zhao, Xiaopeng; Zhang, Shuang; Navarro-Cia, Miguel

DOI:
10.1109/TAP.2019.2927865

Leaky-Wave Antenna with Switchable Omnidirectional Conical Radiation via Polarization Handedness

Yahong Liu, Meize Li, Kun Song, Dingshan Hu, Hongchao Liu, Xiaopeng Zhao, Shuang Zhang, and Miguel Navarro-Cía, *Senior Member, IEEE*

***Abstract*—Reconfigurable antennas capable of beam-steering offer an efficient solution to optimize the use of the crowded wireless medium and can serve as a multifunction antenna. Beam-steering is often achieved by antenna geometry switching at the expense of hardware complexity. Here, polarization is used to realize beam-steering without the need of antenna geometry modification. Depending on the handedness of the feed, backward or forward conical radiation is demonstrated in a ~13λ_0-long short-circuited helically slotted waveguide antenna. Tapering the slit width with a Taylor distribution reduces the measured sidelobe levels by ~3 dB in average and results in a realized gain of 10-13 dB and 11-13 dB for right-handed (backward radiation) and left-handed circularly polarized (forward radiation) feeding, respectively, in the bandwidth from 8.5 to 9.5 GHz.**

***Index Terms*—Beam-steering, circular polarization, helical slit antenna, leaky wave antenna, periodic structure.**

I. Introduction

HELICAL antennas in axial-mode operation are the workhorse of satellite communications because of their immunity to Faraday rotation caused by the ionosphere [1]. In photonics, they have been used to realize negative refraction metamaterials [2], topological metamaterials [3],[4], broadband optical and infrared circular polarizers, absorbers, etc. [5]. When operating in the normal-mode, helical antennas are electrically short monopole antennas with omnidirectional radiation pattern in the plane perpendicular to the helix axis suitable for mobile and portable communication equipment [6] and rocket-borne radiosonde [7]. Helical antennas can also support a conical mode that has found fewer applications in communications, but holds promise for generation of orbital angular momentum [8] and Cherenkov radiation applications [9],[10].

The underlying physics of the conical mode of operation is a leaky-wave [1],[6],[11]. Hence, the beam direction can be steered by sweeping the operating frequency. Although frequency-scanning is used in sensing/radar applications [12]-[15] it is not a desirable feature in modern communication systems, which usually require pattern reconfigurability with fixed frequency operation [16],[17].

A leaky-wave antenna that can provide both frequency-scanning and beam-steering for fixed frequency could be an elegant solution for multifunction radiofrequency systems. Such antenna would facilitate the integration of functionalities by reducing the number of antennas and radiofrequency units to be installed. However, such leaky-wave antenna has not been reported yet in the literature. With this motivation in mind and inspired by work done in the field of metamaterials, we propose a leaky-wave antenna with switchable (front and back semi-infinite planes) omnidirectional conical radiation via polarization handedness. Polarization has been largely overlooked for reconfigurability purposes in microwave engineering, but is well documented at optics for metamaterials [18]. The proposed leaky-wave antenna is a short-circuited helically slotted waveguide antenna (referred as helical tape waveguide, HTW, from now on). A uniform and a tapered HTW to reduce sidelobe levels (SLL) are reported here. Frequency-scanning of 15° (in an 11% fractional bandwidth) is achieved due to the inherent leaky-wave nature of the antenna. The 15° angle scan occurs in the forward/backward direction for left-handed/right-handed circularly-polarized feeding mode.

II. Structural Design

Conventional helical antennas use a metal strip as a radiating element [1]. We will look, however, at their complementary counterpart, the HTW antenna, because it can be fed naturally with a cylindrical waveguide supporting left-handed (LCP) and right-handed circularly-polarized (RCP) modes – such modes are the superposition of the two degenerate TE_{11} modes with spatially orthogonal fields and ±90 deg phase difference, respectively –. Notice that this feeding has not been reported before for helically slotted waveguide antennas

Y. L. is supported by the National Natural Science Foundation of China [Grant Nos. 11874301 and 11204241]; the National Aerospace Science Foundation of China [Grant No. 2016ZF53061]; the Natural Science Basic Research Plan in Shaanxi Province of China [Grant No. 2017JM1009]; the Fundamental Research Funds for the Central Universities [Grant No. 3102017jghk02004]; K. S. acknowledges support from the National Natural Science Foundation of China [Grant No. 61601375]. S. Z. acknowledges support from European Research Council Consolidator Grant (TOPOLOGICAL); the Royal Society and the Wolfson Foundation; and Horizon 2020 Action, Project Nos. 734578 (D-SPA) and 648783. M. N.-C. acknowledges support from University of Birmingham [Birmingham Fellowship]. (*Corresponding authors: Yahong Liu and Miguel Navarro-Cía*)

Y. Liu, M. Li, K. Song, D. Hu and X. Zhao are with the Department of Applied Physics, Northwestern Polytechnical University, Xi'an, 710129, China (e-mail: yhliu@nwpu.edu.cn).

H. Liu, S. Zhang and M. Navarro-Cía, are with the School of Physics and Astronomy, University of Birmingham, Birmingham B15 2TT, United Kingdom (e-mail: m.navarro-cia@bham.ac.uk).

[7],[19], except in our previous work devoted to polarization-induced waveguide filtering and orbital angular momentum beam generation [20]. Unlike Ref. [20], the HTW is terminated in a short circuit to enable leaky-wave functionality for both RCP and LCP. For leaky-wave radiation to occur, the waveguide modes must have opposite handedness to the helix. The waveguide mode that initially has the same handedness (RCP in this work) travels until the end of the HTW and, upon reflection by the terminated mirror, turns into the opposite handedness to the helix, which can radiate into free space. This will be illustrated subsequently in III. Results and Discussion. The dispersion diagram of this short-circuited HTW antenna calculated via the ABCD matrix method [21] can be found in the Appendix. The same concept of handedness matching upon reflection has been exploited for optical tractor beam applications [22].

Two HTW antennas are designed and fabricated with constant pitch a = 20 mm (~0.6λ_0, where λ_0 is the free-space wavelength), diameter d = 21.6 mm (~0.65λ_0) and physical length l = 430 mm (~13λ_0). The pitch angle is $\psi = \arctan(a/\pi d)$ = 16.4°. The helix tape is made of copper with thickness t = 0.5 mm and wraps a circular resin tube (i.e. hollow cylinder). One HTW antenna is based on a uniform slit of width s = 5 mm (Fig. 1(a)), chosen so that approximately 90-95% of the power is radiated [11]. With such uniform slit, the leakage constant α does not change along the length of the HTW, and the aperture distribution has an exponential amplitude variation and a constant phase. Such an aperture distribution results in a high sidelobe level. To reduce sidelobes for both LCP and RCP modes, thereby yielding higher main lobe gain, the second HTW antenna has a tapered slit width $s(z)$ (Fig. 1(b)). Unlike monofilar axial-mode helical antennas [1], the HTW antenna leakage characteristics in the conical mode operation are very sensitive to even moderate changes in dimensions [20], and thus, the effect of moderate departures from uniformity is large. This greatly facilitates the realization of the taper with a Taylor amplitude distribution for the leakage constant α.

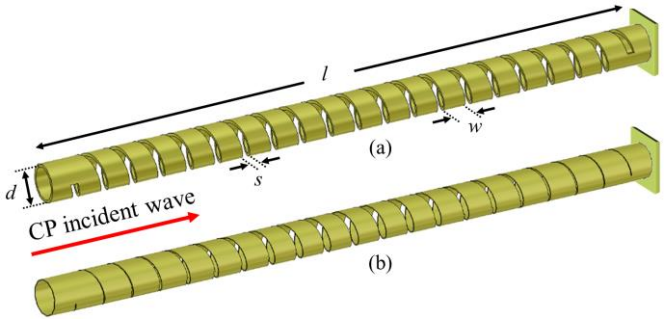

Fig. 1. Sketch of the 20-turn uniform (a) and tapered (b) HTW antenna. The uniform HTW has constant slit width, metallic width and thus lattice constant of s = 5 mm, w = 15 mm, and $a = s + w$ = 20 mm, respectively. The tapered HTW antenna keep constant the spacing between turns a = 20 mm, while s and w vary. The dimension of the mirror is 26 × 26 × 0.5 mm^3.

The procedure to find out the leakage constant $\alpha(z)$ for the non-uniform HTW relies on the ABCD matrix method [21] and assumes that the local periodicity approximation holds. This assumption is reasonable here given the adiabatic Taylor distribution envisioned for the non-uniform HTW. Several uniform HTWs are simulated with constant a and d, but different s to find the required value of α for the Taylor distribution. Notice that the circular resin tube is not considered in this design procedure and that metal is modelled as a perfect electric conductor. Hence, the attenuation computed via the ABCD matrix method is indeed the leakage constant and is identical for LCP and RCP modes. The effect of the circular resin tube and dielectric absorption in the radiation characteristics are discussed in the Appendix. Alternatively, the leakage constant could have been calculated as $\alpha = -\frac{1}{2l} ln\left(\frac{P(l)}{P(0)}\right)$, where $P(l)$ is the power remaining in the waveguide at a distance $z = l$ along the length of the HTW and $P(0)$ is the power input at z = 0 [20]. The calculated frequency-dependent leakage constant $\alpha(z)$ for the uniform and non-uniform HTW antenna can be found in Fig. 2. The corresponding $s(z)$ at the beginning of each turn can be found in the Appendix.

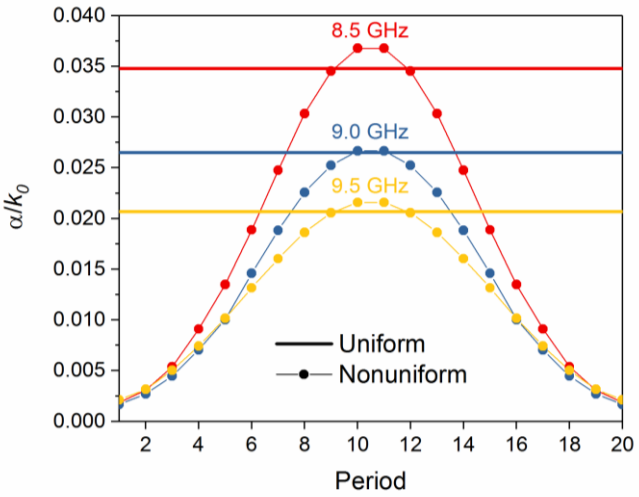

Fig. 2. Simulated leakage constant $\alpha(z)$ for uniform and non-uniform slit width.

III. Results and Discussion

A. Underlying mechanism and S_{11}

Prior to the measurements, the leaky-wave and polarization switch-ability characteristics of the proposed HTWs can be demonstrated unequivocally with the full-wave simulations. Figure 3 displays the electric field distribution of the two HTW antennas. For the LCP feeding, the energy leaks through the slits with a conical radiation pattern akin to the HTW without mirror [16] and Bull's Eye antennas [23]-[27]. For RCP feeding, the energy travels first along the waveguide almost unperturbedly and after reflecting on the end mirror starts leaking through the silts as it travels toward the feeding with a conical radiation pattern opposite to the LCP feeding. Hence, a standing-wave pattern is observed inside the HTW under RCP feeding unlike the LCP case.

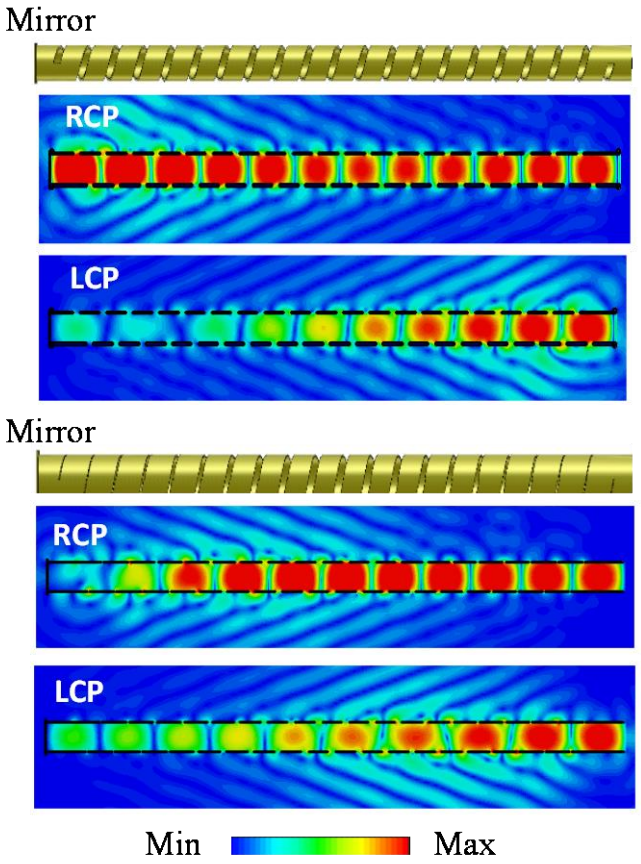

Fig. 3. Simulated electric field distributions for RCP and LCP feeding at 9 GHz: (top) Uniform and (bottom) non-uniform leaky-wave antennas.

Figure 4 shows the measured reflection coefficient S_{11} for both HTW designs under the two circular polarization handedness. The reflection coefficient is plotted from 8.4 GHz upwards since the cutoff frequency of the circular waveguide feeding the HTW antennas is 8.14 GHz. The reflection coefficient for the uniform HTW antenna is below -20 dB for both LCP and RCP feeding. Tapering the slit width worsen the S_{11}, which however still remains below -10 dB in the spectral window shown for both LCP and RCP feeding. Simulations are in reasonable agreement with the measurements given that the full setup and the circular resin tube are not modelled as illustrated in Fig. 8 of the Appendix.

B. Radiation characteristics

For small *s*, the mode with opposite handedness to that of the helix (RCP feeding here) travels unperturbedly along the HTW before being reflected. However, for moderate values of *s* such as 5 mm (~0.15λ_0), this mode can also leak before being reflected by the end mirror. This can be observed indeed in the top contour plots of Fig. 5 where the numerically-computed realized gain is plotted as a function of frequency and radiation angle for the uniform HTW antenna. For RCP (Fig. 5(b)), the main lobes emerge near -70° and 70°. Two prominent sidelobes appear near -110° and 110°. Since these angles are exactly those observed for the main lobes with LCP feeding (Fig. 5(a)), we can conclude that they are residual leakage radiation of the RCP mode as it travels from the generator toward the end of the waveguide. Further evidence supporting this conclusion comes from the observation that the LCP case does not have any prominent sidelobes near -70° and 70°; for LCP feeding negligible energy reaches the end of the waveguide and is reflected back to generate such sidelobes.

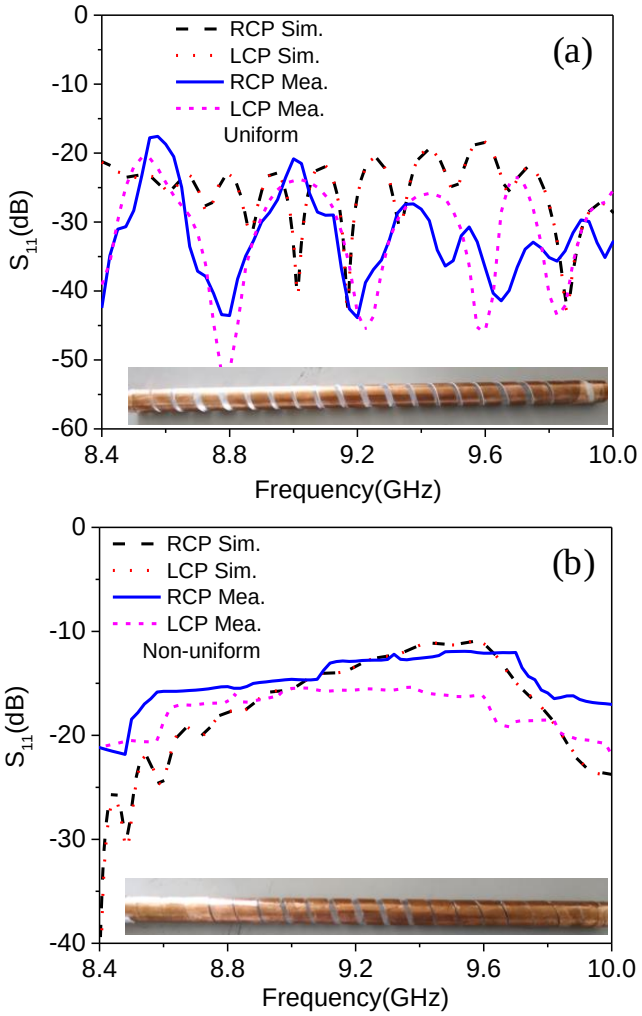

Fig. 4. Reflection coefficient under RCP and LCP feeding for (a) uniform and (b) non-uniform HTW antenna. Insets: picture of the fabricated samples.

When comparing Fig. 5(a) with Fig. 5(b), one can perceive the benefits of the taper. Firstly, the prominent sidelobes for RCP feeding near -110° and 110° are significantly reduced. The Taylor distribution is not meant to address this; this reduction is a byproduct of using consistently smaller *s* than 5 mm, except for the two central turns. Secondly, the overall background level is reduced. Even though the non-uniform HTW antenna has a worse S_{11} than the uniform one, it displays higher realized gain for both polarizations due to the significant sidelobe level and background reduction achieved with the Taylor taper.

To facilitate the comparison with measurements – done in an anechoic chamber with an AV 3629 vector network analyzer, and a linearly polarized horn antenna (1-18 GHz) –, Fig. 6 presents the far-field radiation patterns in polar form for the uniform and non-uniform HTW antennas at the

representative frequencies of 8.5 GHz, 9 GHz and 9.5 GHz. Overall, simulations agree well with measurements for all cases.

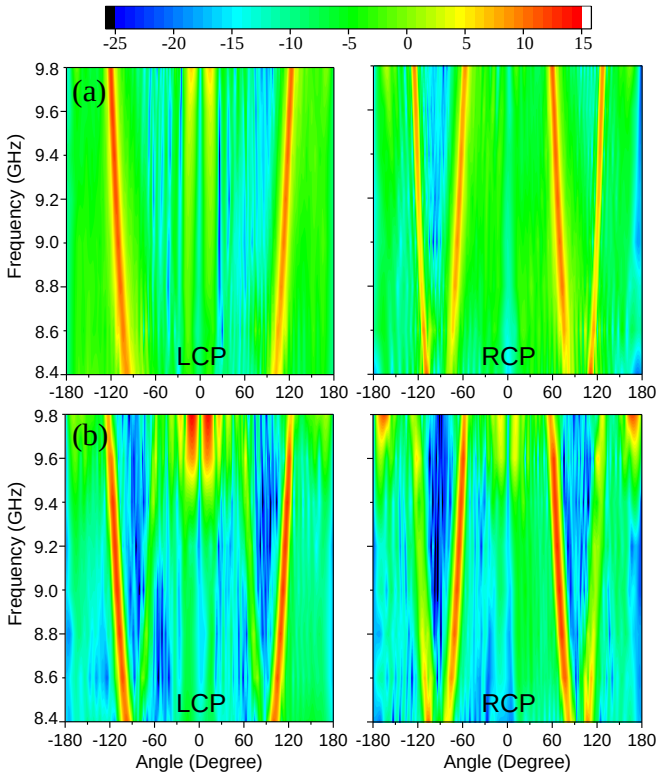

Fig. 5. Realized gain in dB vs. radiation angle and frequency for LCP (left) and RCP (right) feeding: (a) Uniform and (b) non-uniform HTW antenna.

The simulated main lobe gains for the uniform HTW antenna are 11.4 dB and 11.7 dB at 113° and 246° (-114°) for LCP feeding at the central frequency of 9 GHz (left-hand side of Fig. 6(a)). The measured counterparts are 11.1 dB and 11.1 dB at 115° and 250° (-110°) (left-hand side of Fig. 6(c)). For RCP feeding, the main lobe gains are 11.3 dB and 11.6 dB at 67° and 294° (-66°) according to the simulation (right-hand side of Fig. 6(a)), and 11.4 dB and 8.9 dB at 66° and 294° (-66°) according to the measurement (right-hand side of Fig. 6(c)).

As anticipated from Fig. 5, gain levels increase for the non-uniform HTW antenna despite its worse S_{11}. At 9 GHz, the simulated main lobe gains go up to 10.6 dB (111°) and 12.5 dB (249° = -111°) for LCP feeding, and 11.3 dB (69°) and 11.2 dB (292° = -68°) for RCP feeding (Fig. 6(b)). The measured counterparts (Fig. 6(d)) are 11.8 dB (115°) and 12.6 dB (250° = -110°) for LCP feeding, and 12.1 dB (68°) and 10.5 dB (294° = -66°) for RCP feeding.

Similar results are obtained at the frequencies of 8.5 GHz and 9.5 GHz. Hence, they are all tabulated in Table I along with the sidelobe levels. Notice that the tabulated gain is the average gain between the two measured main lobes, whereas the SLL represents the worst case (i.e. the sidelobe level with respect to the minimum gain of either of the two main lobes). The general gain reduction for RCP compared to LCP reported in Table I can arguably link to the additional dissipation loss that the RCP mode experienced, as it has to travel an extra l = 430 mm distance before being able to radiate.

TABLE I
MEASURED RADIATION PATTERN CHARACTERISTICS

Freq. (GHz)	Forward Beam (LCP)				Backward Beam (RCP)			
	Average Gain (dB)		SLL (dB)		Average Gain (dB)		SLL (dB)	
	uni.	non.	uni.	non.	uni.	non.	uni.	non.
8.5	10.8	11.5	-15.8	-19.3	10.9	10.7	-5.7	-8.3
9.0	11.1	12.2	-14.5	-17.3	10.2	11.3	-12	-11.3
9.5	11.3	12.6	-10.1	-17.1	10.3	12	-8.5	-12.5

Similar conical radiation is achieved with Bull's Eye [23]-[29], and Fabry-Perot antennas [30],[31], albeit, for the reported implementation of those antennas so far, in half of the radiation space without the ability to switch radiation to the other half-space. Setting aside this key aspect, the reported maximum gains of the above-mentioned antennas [23]-[31] overpass the one reported here, but the frequency-scanning within 3 dB scan losses are similar in all cases.

IV. Conclusion

To conclude, we have designed and fabricated two leaky-wave antennas based on a short-circuited HTW with a uniform and non-uniform slit operating in the X band. In addition to a frequency-scanning of 15° (in a 11% fractional bandwidth) – 23° in a 17.3% fractional bandwidth if considering the simulations not shown here –, we have demonstrated numerically and experimentally that the radiation direction of the proposed antennas can be switched with the polarization of the feeding. As the LCP mode is incident into the proposed antennas, the power largely leaks through the slits and leads to forward leakage radiation with conical pattern with a measured gain ranging from 11 to 12 dB for the uniform case, and 11-13 dB for the non-uniform case. As the RCP mode is incident on the proposed leaky-wave antenna, the power largely leaks through the slits into a backward conical radiation pattern with a measured gain ranging from 9 to 11 dB for the uniform case, and 10-13 dB for the non-uniform case. The reconfigurability of the proposed HTW antennas without additional hardware complexity and their simple waveguide design make them attractive for the next generation of communication and sensing systems at (sub-)millimeter-waves.

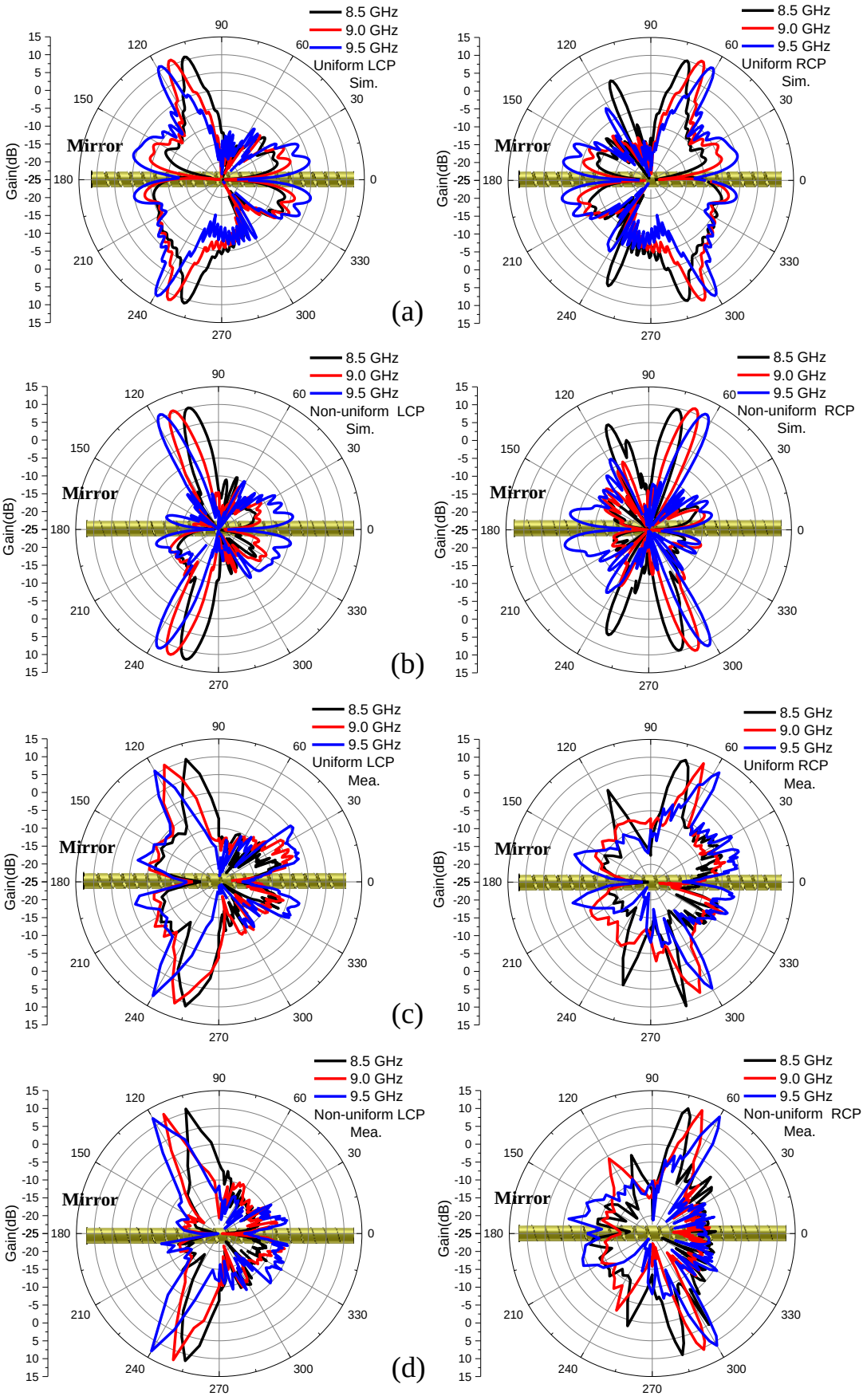

Fig. 6. (a) Far-field radiation patterns at different frequencies for LCP (left) and RCP (right) incident waveguide mode. Simulated (a) uniform and (b) non-uniform leaky-wave HTW antennas, and measured (c) uniform and (d) non-uniform leaky-wave HTW antennas.

APPENDIX

A. *Dispersion diagram*

The complex dispersion diagram shown below (Fig. 7) is computed with the frequency-domain solver of CST Microwave Studio® and using the ABCD matrix method from a single unit cell and with a macro-cell made up of 2, 3 and 5 unit cells to [21]. More technical details about the simulation can be found in Appendix B. Figure 7 reveals that the phase constant is more robust against changes in *s* than the leakage constant. This facilitates the design of the non-uniform HTW antenna since we can assume that each period will radiate at almost the same angle. Indeed, the maximum deviation expected for the radiation angle due to the range of propagation constants for *s*(z) is 2.5°, 1.5° and 1.2° at 8.5, 9 and 9.5 GHz, respectively. Specifically, for 9 GHz, this dispersion diagram predicts the main lobes to emerge between 114.9°/245.1° and 116.4°/243.6° for LCP, whereas for RCP they are expected between 63.6°/294.9° and 65.1°/296.4°, which agree very well with the time-domain simulations of the fabricated samples and the measurements.

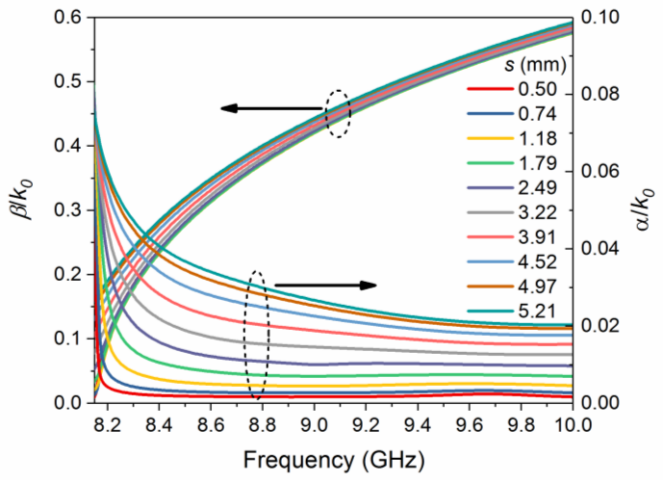

Fig. 7. Dispersion diagram of the short-circuited HTW antenna along with the light line.

B. *Simulations*

We use the commercial software CST Microwave Studio® to design and model the HTW antennas. Both, frequency-domain and transient solvers are used for the results reported here. The Eigen-mode solver is also used for validation purposes, but its results are not reported. Notice that the coaxial-to-rectangular transition and the rectangular-to-circular transition used in the measurements (Fig. 8) are not modelled numerically with either of the solvers, which may be the reason of the minor disagreements between simulations and measurements in Figs. 4 and 6. Open boundary conditions are applied to the *x*-, *y*-, and *z*-directions. Metal is modelled as a perfect electric conductor. Given the 0.22 mm thick resin tube's small electrical thickness (~0.007λ_0), it is considered unnecessary to model the tube in the simulations for the main body of the manuscript such to reduce computational burden. Indeed, such negligible influence is demonstrated in Table II where the radiation pattern characteristics with and without lossy resin tube (ε = 2.2 - j0.001) are tabulated. The solver's adaptive mesh (tetrahedral and hexahedral in the frequency- and time-domain solvers, respectively) is employed with a convergence accuracy of the S-parameters of 0.001.

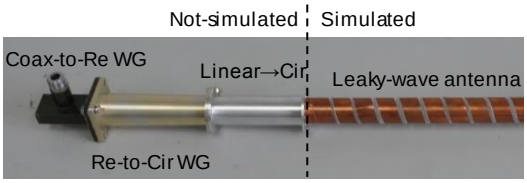

Fig. 8. Picture of the measured prototype highlighting the simulated section.

TABLE II
SIMULATED RADIATION PATTERN CHARACTERISTICS WITH AND WITHOUT LOSSY RESIN TUBE

FREQ. (GHz)	FORWARD BEAM (LCP)				BACKWARD BEAM (RCP)			
	Average Gain (dB)		SLL (dB)		Average Gain (dB)		SLL (dB)	
	w/	w/o	w/	w/o	w/	w/o	w/	w/o
8.5	11.4	11.3	-27.5	-28.0	9.7	9.7	-26.5	-27.0
9.0	12.1	11.6	-15.9	-15.6	11.4	11.3	-15.0	-15.6
9.5	12.3	11.7	-10.9	-11.3	11.6	11.3	-11.4	-11.3

C. *Slit width dimensions for the tapered HTW antenna*

TABLE III
SLIT WIDTH AT THE BEGINNING OF EACH PERIOD

TURN	Slit width (mm)
1, 20	0.5
2, 19	0.74
3, 18	1.18
4, 17	1.79
5, 16	2.49
6, 15	3.22
7, 14	3.91
8, 13	4.52
9, 12	4.97
10, 11	5.21

REFERENCES

[1] J. D. Kraus, and R. J. Marhefka, *Antennas: For All Applications*, 3rd ed. New York, NY, USA: McGraw-Hill, 2002.

[2] J. B. Pendry, "A Chiral Route to Negative Refraction," *Science*, vol. 306, no. 5700, pp. 1353-1355, Nov. 2004, 10.1126/science.1104467

[3] W. Gao, M. Lawrence, B. Yang, F. Liu, F. Fang, B. Béri, J. Li, and S. Zhang, "Topological Photonic Phase in Chiral Hyperbolic Metamaterials," *Phys. Rev. Lett.*, vol. 114, no. 3, pp. 037402-1-5, Jan. 2015, 10.1103/PhysRevLett.114.037402

[4] B. Yang, Q. Guo, B. Tremain, L. E. Barr, W. Gao, H. Liu, B. Béri, Y. Xiang, D. Fan, A. P. Hibbins, and S. Zhang , "Direct observation of topological surface-state arcs in photonic metamaterials," *Nature Comm.*, vol. 8, 97, Jul. 2017, 10.1038/s41467-017-00134-1

[5] J. Kaschke, and M. Wegener, "Optical and Infrared Helical Metamaterials," *Nanophoton.*, vol. 5, no. 4, pp. 510-523, 2016, 10.1515/nanoph-2016-0005

[6] C. A. Balanis, *Antenna Theory: Analysis and Design*, 3rd ed.

Hoboken, NJ, USA: John Wiley & Sons, 2005.

[7] S. W. Thompson, and E. R. Farley, "Slotted Cylinder Antennas For Radiosonde Set AN/DMQ-6," United States Army, Electron. Res. Develop. Lab., Fort Monmouth, NJ, USA, Tech. Rep. 2368, Sept. 1963.

[8] J. Wang, J.-Y. Yang, I. M. Fazal, N. Ahmed, Y. Yan, H. Huang, Y. Ren, Y. Yue, S. Dolinar, M. Tur, and A. E. Willner, "Terabit free-space data transmission employing orbital angular momentum multiplexing," *Nature Photon*., vol. 6, no.7, pp. 488-496, 2012, 10.1038/nphoton.2012.138

[9] J. Soln, "Helical Cerenkov effect, a novel radiation source," *IEEE Trans. Plasma Sci.*, vol. 22, no. 5, 526-529, Oct. 1994, 10.1109/27.338263

[10] J. Soln, "The helical Cerenkov effect with a non-monoenergetic electron beam," *J. Phys. D: Appl. Phys.*, vol. 30, no. 21, 2936-2945, Jul. 1997, 10.1088/0022-3727/30/21/006

[11] D. R. Jackson, and A. A. Oliner, "Leaky-Wave Antennas," in *Modern Antenna Handbook*. Hoboken, NJ, USA: Wiley-Blackwell, Nov. 2007.

[12] F. S. Johansson, L. G. Josefsson, and T. Lorentzon, "A novel frequency-scanning reflector antenna," *IEEE Trans. Antennas Propag.*, vol. 37, no. 8, pp. 984-989, Aug. 1989, 10.1109/8.34134

[13] S.-T. Yang, and H Ling, "Design of a Microstrip Leaky-Wave Antenna for Two-Dimensional Bearing Tracking," *IEEE Antennas Propag. Lett.*, vol. 10, pp. 784-787, Aug. 2011, 10.1109/LAWP.2011.2163377

[14] S.-T. Yang, and H. Ling, "Application of a Microstrip Leaky Wave Antenna for Range-Azimuth Tracking of Humans," *IEEE Geosci. Remote Sens. Lett.*, vol. 10, no. 6, pp. 1384-1388, Nov. 2013, 10.1109/LGRS.2013.2243401

[15] Y. Álvarez, R. Camblor, C. García, J. Laviada, C. Vázquez, S. Ver-Hoeye, G. Hotopan, M. Fernández, A. Hadarig, A. Arboleya, F. Las-Heras, "Submillimeter-Wave Frequency Scanning System for Imaging Applications," *IEEE Trans. Antennas Propag.*, vol. 61, no. 11, pp. 5689-5696, Nov. 2013, 10.1109/TAP.2013.2275747

[16] Y. Jay Guo, P.-Y. Qin, S.-L. Chen, W. Lin, and R. W. Ziolkowski, "Advanced in Reconfigurable Antenna Systems Facilitated by Innovative Technologies," *IEEE Access*, vol. 6, pp. 5780-5794, Jan. 2018, 10.1109/ACCESS.2017.2789199

[17] Md. A. Towfiq, I. Bahceci, S. Blanch, J. Romeu, L. Jofre, and B. A. Cetiner, "A Reconfigurable Antenna With Beam Steering and Beamwidth Variability for Wireless Communications," *IEEE Trans. Antennas Propag.*, vol. 66, no. 10, pp. 5052-5063, Oct. 2018, 10.1109/TAP.2018.2855668

[18] L. Huang, S. Zhang, and T. Zentgraf, "Metasurface holography: from fundamentals to applications," *Nanophotonics*, vol. 7, no. 6, pp. 1169-1190, Mar. 2018, 10.1515/nanoph-2017-0118

[19] Y.-H. Yang, J.-L. Guo, B.-H. Sun, and Y.-H. Huang, "Dual-Band Slot Helix Antenna for Global Positioning Satellite Applications," *IEEE Trans. Antennas Propag.*, vol. 64, no. 12, pp. 5146-5152, Dec. 2016, 10.1109/TAP.2016.2623647

[20] Y. Liu, Q. Guo, H. Liu, C. Liu, K. Song, B. Yang, Q. Hou, X. Zhao, S. Zhang, and M. Navarro-Cía, "Circular-Polarization-Selection Transmission Induced by Spin-Orbit Coupling in a Helical Tape Waveguide," *Phys. Rev. Appl.*, vol. 9, no. 5, pp. 054033-1-7, 2018, 10.1103/PhysRevAppled.9.054033

[21] G. Valerio, S. Paulotto, P. Baccarelli, P. Burghignoli, and A. Galli, "Accurate Bloch analysis of 1-D periodic lines through the simulation of truncated structures," *IEEE Trans. Antennas Propag.*, vol. 59, no. 6, pp. 2188–2195, June 2011, 10.1109/TAP.2011.2143667

[22] D. E. Fernandes, and M. G. Silveirinha, "Optical tractor beam with chiral light," *Phys. Rev. A*, vol. 91, no. 6, pp.061801-1-6, Jun. 2015, 10.1103/PhysRevA.91061801

[23] U. Beaskoetxea, M. Navarro-Cía, and M. Beruete, "Broadband frequency and angular response of a sinusoidal bull's eye antenna," *J. Phys. D: Appl. Phys.*, vol. 49, no. 26, 265103-1-6, May 2016, 10.1088/0022-3727/49/26/265103

[24] C. J. Vourch, B. Allen, and T. D. Drysdale, "Planar millimetre-wave antenna simultaneously producing four orbital angular momentum modes and associated multi-element receiver array," *IET Microw. Antennas Propag.*, vol. 10, no. 14, pp. 1492-1499, Nov. 2016, 10.1049/iet-map.2015.0808

[25] U. Beaskoetxea, S. Maci, M. Navarro-Cía, and M. Beruete, "3-D Printed 96 GHz Bull's Eye Antenna with Off-Axis Beaming," *IEEE Trans. Antennas Propag.*, vol. 65, no. 1, pp. 17-25, Jan. 2017, 10.1109/TAP.2016.2628322

[26] D. Comite, V. Gómez-Guillamón Buendía, S. K. Podilchak, D. Di Ruscio, P. Baccarelli, P. Burghignoli, and A. Galli, "Planar Antenna Design for Omnidirectional Conical Radiation Through Cylindrical Leaky Waves," *IEEE Antennas Wireless Propag. Lett.*, vol. 17, no. 10, pp. 1837-1841, Oct. 2018, 10.1109/LAWP.2018.2867829

[27] D. Comite, W. Fuscaldo, S. K. Podilchak, P. D. Hilario Re, V. Gómez-Guillamón Buendía, P. Burghignoli, P. Baccarelli and A. Galli, "Radially Periodic Leaky-Wave Antenna for Bessel Beam Generation Over a Wide-Frequency Range," *IEEE Trans. Antennas Propag.*, vol. 66, no. 6, pp. 2828-2843, Jun 2018, 10.1109/TAP.2018.2823862

[28] U. Beaskoetxea, and M. Beruete, "High Aperture Efficiency Wide Corrugations Bull's-Eye Antenna Working at 60 GHz," *IEEE Trans. Antennas Propag.*, vol. 65, no. 6, pp. 3226-3230, Jun. 2017, 10.1109/TAP.2017.2696423

[29] C. J. Vourch, and T. D. Drysdale, "V-band Bull's eye antenna for multiple discretely steerable beams," *IET Microw. Antennas Propag.*, vol. 10, no. 3, pp. 315-328, 2016, 10.1049/iet-map.2015.0425

[30] P. Burghignoli, G. Lovat, F. Capolino, D. R. Jackson, and D. R. Wilton, "Highly Polarized, Directive Radiation From a Fabry-Pérot Cavity Leaky-Wave Antenna Based on a Metal Strip Grating," *IEEE Trans. Antennas Propag.*, vol. 58, no. 12, pp. 3873-3883, Dec. 2010, 10.1109/TAP.2010.2078441

[31] J. Ren, W. Jiang, K. Zhang, and S. Gong, "A High-Gain Circularly Polarized Fabry–Perot Antenna with Wideband Low-RCS Property," *IEEE Antennas Wireless Propag. Lett.*, vol. 17, no. 5, pp. 853-856, May 2018, 10.1109/LAWP.2018.2820015

Yahong Liu received the B.S. degree in the School of Aeronautics from Northwestern Polytechnical University, Xi'an, China, in 2003. She received M.S. degree and Ph.D. degree in the Department of Applied Physics from Northwestern Polytechnical University, Xi'an, China, in 2006 and 2010, respectively. Currently, she is an associate professor in the Department of Applied Physics, Northwestern Polytechnical University, China. She was a Visiting Scholar with the University of Birmingham, Birmingham, United Kingdom, from Dec. 2016 to Nov. 2017. Her research interests are topological materials,

electromagnetic metamaterials, applications of metamaterial concepts including microwave antennas and perfect absorbers.

Meize Li received the B.S. degree in the Department of Physics from Yuncheng university, Shanxi, China, in 2017. Currently, she is studying in the Department of Applied Physics in Northwestern Polytechnical University, Xi'an, China, towards the M.S. degree. Her research interest is electromagnetic metamaterials.

Kun Song was born in Shandong Province, China, in 1984. He received B.S. and Ph.D. degrees in the Department of Applied Physics from Northwestern Polytechnical University, Xi'an, China, in 2008, and 2014, respectively. Currently, he is an assistant professor in the Department of Applied Physics, Northwestern Polytechnical University, Xi'an, China. His research interests include chiral metamaterials, information optics, and metasurfaces.

Dingshan Hu received the B.S. degree in the Department of Applied Physics from Northwestern Polytechnical University, Xi'an, China, in 2018. Currently, he serves as an engineer in a company.

Hongchao Liu received the B.S. degree from Beijing Normal University, Beijing, China, in 2010, and the Ph.D. degree from the Department of Physics, Hong Kong University of Science and Technology, Hong Kong, China, in 2014. He is currently a Research Fellow with the School of Physics and Astronomy, University of Birmingham, United Kingdom. His research interests include metamaterials, information optics, and topological materials.

Xiaopeng Zhao was born in Yulin, Shaanxi, China, in 1957. He is currently a professor in the Department of Applied Physics, Northwestern Polytechnical University, Xian, China. In 1979, he graduated from the Department of Physics of Lanzhou University in Lanzhou, China, and received the B.S. degree. He received the Ph.D degree in Material Physics from Institute of Metal Research, Chinese Academy of Sciences, Shenyang, China, in 1995. His research has led to 290 publications and 93 Chinese patents. His current research interests include Biomimetical Materials, Intelligent Materials and Structure, Optics, Nanotechnology, and Metamaterials.

He was awarded Special Government Allowance by the State Council, Young and Middle-aged Expert with outstanding contributions to the national defense technology industry.

Shuang Zhang received the B.S degree in Physics from Jilin University, China, in 1993, and received the M.S. degree in Physics from Northeastern University, in 1999. He received the Ph.D. degree in Electrical Engineering from University of New Mexico in 2005.

He was a Postdoctoral Associate with the University of Illinois at Urbana Champaign, and the University of California, Berkeley, Jan 2006 – Aug 2006, and Aug 2006 – Aug 2009, respectively. From Aug 2009 to March 2010, he was a Research Assistant Engineer with the University of California, Berkeley. He was appointed a Reader with the University of Birmingham, UK, in 2010 and promoted to full Professor in 2013. His current research interests include Nano- and terahertz photonics, metamaterials, nonlinear optics, optoelectronics, nano-fabrications, and topological photonics.

He was awarded IUPAP (International Union of Pure and Applied Physics) Young Scientist Prize in Optics in 2010, and Royal Society Wolfson Award in 2016. He was elected Fellow of OSA in 2016. He serves as an editor for the Journal of Light: Science & Applications, and for Advanced Photonics.

Miguel Navarro-Cía (S'08–M'10–SM'15) was born in Pamplona, Spain, in 1982. He received the MEng and PhD degrees in Telecommunication Engineering, and MRes degree in Introduction to Research in Communications from the Universidad Pública de Navarra, Spain, in 2006, 2010, and 2007, respectively.

From 2006 to 2010, he was a Pre-Doctoral Researcher (FPI Fellowship recipient) with the Electrical and Electronic Engineering Department, Universidad Pública de Navarra, where he was also a Research and Teaching Assistant from 2010 to 2011. He was a Research Associate with Imperial College London, London, U.K., in 2011 and at University College London, in 2012, and a Junior Research Fellow with Imperial College London, from 2012 to 2015. Currently, he is a Birmingham Fellow with the School of Physics and Astronomy, University of Birmingham, Birmingham, U.K. He is also affiliated as a Visiting Researcher with Imperial College London and University College London. He was a Visiting Researcher with the University of Pennsylvania, Philadelphia, PA, USA, for three months in 2010, with Imperial College London in 2008, 2009, and 2010 for four, six, and three months, respectively, and with the Valencia Nanophotonics Technology Center, Valencia, Spain, for two months in 2008. His current research interests include plasmonics, near-field time-domain spectroscopy/microscopy, metamaterials, antennas and frequency-selective surfaces at millimeter-wave, terahertz, and infrared.

Dr. Navarro-Cía is a Senior Member of the Optical Society of America and a Member of the Institute of Physics. He was a recipient of the Best Doctoral Thesis in Basic Principles and Technologies of Information and Communications, and Applications corresponding to the XXXI Edition of Awards Telecommunication Engineers 2010 and twice the CST University Publication Award for the best international journal publication using CST Microwave Studio (in 2012 and 2016). He was also a recipient of the 2011 Junior Research Raj Mittra Travel Grant.